SCIENCE CHINA
Physics, Mechanics & Astronomy

•Article•
Editor's Focus

March 2021 Vol. 64 No. 3: 234263
https://doi.org/10.1007/s11433-020-1637-8

Editor's Focus

Microdisk lasers on an erbium-doped lithium-niobite chip

Qiang Luo[1], ZhenZhong Hao[1], Chen Yang[1], Ru Zhang[1], DaHuai Zheng[1], ShiGuo Liu[1], HongDe Liu[1], Fang Bo[1,2,3*], YongFa Kong[1*], GuoQuan Zhang[1*], and JingJun Xu[1*]

[1] *MOE Key Laboratory of Weak-Light Nonlinear Photonics, TEDA Institute of Applied Physics and School of Physics, Nankai University, Tianjin 300457, China;*
[2] *Collaborative Innovation Center of Extreme Optics, Shanxi University, Taiyuan 030006, China;*
[3] *Collaborative Innovation Center of Light Manipulations and Applications, Shandong Normal University, Jinan 250358, China*

Received October 5, 2020; accepted October 31, 2020; published online December 2, 2020

Lithium niobate on insulator (LNOI) provides a platform for the fundamental physics investigations and practical applications of integrated photonics. However, as an indispensable building block of integrated photonics, lasers are in short supply. In this paper, erbium-doped LNOI laser in the 1550-nm band was demonstrated in microdisk cavities with high quality factors fabricated in batches by UV exposure, inductively coupled plasma reactive ion etching, and chemomechanical polishing. The threshold and conversion efficiency of the erbium-doped LNOI microdisk laser were measured to be lower than 1 mW and 6.5×10^{-5}%, respectively. This work will benefit the development of integrated photonics based on LNOI.

lithium niobite, LNOI, microcavities, laser

PACS number(s): 42.55.Sa, 42.55.Rz, 77.84.Bw, 77.55.+f

Citation: Q. Luo, Z. Z. Hao, C. Yang, R. Zhang, D. H. Zheng, S. G. Liu, H. D. Liu, F. Bo, Y. F. Kong, G. Q. Zhang, and J. J. Xu, Microdisk lasers on an erbium-doped lithium-niobite chip, Sci. China-Phys. Mech. Astron. **64**, 234263 (2021), https://doi.org/10.1007/s11433-020-1637-8

1 Introduction

As an excellent optical crystal material, lithium niobate (LN) has advantages such as a small absorption coefficient (0.02 cm^{-1} at 1064 nm); wide transparent window (0.35-5 μm); high nonlinear coefficient (d_{33}=−41.7 pm/V); and good electro-optic (r_{33}=32.2 pm/V) [1], acousto-optic, and photorefractive effects. Benefiting from the commercial production of LN on insulator (LNOI), the research on LNOI integrated optical devices has increased explosively. For example, Lin et al. [2] fabricated the first LNOI microdisk cavity using femtosecond laser micromachining, followed by focused ion beam milling. Subsequently, an inductively coupled plasma reactive ion etching (ICP-RIE) process was introduced to prepare LNOI microdisk cavity [3] and combined with photolithography to achieve batch production [4]. With the assistance of chemomechanical polishing (CMP), the quality (Q) factors of LNOI microdisk cavities have been recently improved up to 10^7 [5,6], and the propagating loss of the LNOI waveguide has been reduced to as low as 0.027 dB/cm [7]. Using the nonlinearity of LN, various nonlinear optical effects, including sum frequency generation, second harmonic generation, difference frequency generation, and four-wave mixing, have been realized in LNOI microdisks, microrings, and waveguides [8-17]. Integrated LN electro-optic modulators with high operating frequencies and CMOS-compatible voltages have also been designed [18]. Subsequently, Cai's group [19] designed an electro-optic modulator on the basis of a silicon-LN hybrid

*Corresponding authors (Fang Bo, email: bofang@nankai.edu.cn; YongFa Kong, e-mail: kongyf@nankai.edu.cn; GuoQuan Zhang, email: zhanggq@nankai.edu.cn; JingJun Xu, email: jjxu@nankai.edu.cn)

integrated platform, with a modulation bandwidth of more than 70 GHz and a modulation rate of 112 Gbit/s. To achieve high-efficiency coupling between off-chip and on-chip LNOI devices, grating couplers [20,21] and tapered waveguides or tapered fibers were introduced into the system, and coupling efficiency up to 73.8% [22,23] was reported.

Generally, an integrated optical system includes light sources, detectors, and devices with transmission and control functions. However, no laser on LNOI has been reported. Some efforts have been made to study LNOI devices doped with rare-earth ions. The optical properties of Er^{3+}-, Tm^{3+}-, and Yb^{3+}-doped LNOI have been investigated [24-26]. However, due to the limitation of the concentration of ion implantation or the low quality of the integrated devices, lasers on LNOI chips are in short supply.

In this paper, we fabricated on-chip erbium-doped LN microdisk cavities with high Q factors (1.26×10^6) using UV lithography, inductively coupled plasma reactive ion etching (ICP-RIE), and chemical-mechanical polishing (CMP) techniques. A 1550-nm band laser output was observed under light pump in the 980-nm band. The laser threshold is as low as 292 μW, and the conversion efficiency is 6.5×10^{-5}%.

2 Fabrication and characterization of erbium-doped LNOI microdisks

We fabricated erbium-doped microdisk cavities on an erbium-doped Z-cut LNOI wafer with a doping concentration of ~0.1 mol%. The thickness of the erbium-doped LN film, silicon-dioxide buffer layer, and silicon substrate were 0.6, 2, and 500 μm, respectively. Figure 1 illustrates the fabrication process of erbium-doped LNOI microdisk cavities, which are mainly divided into eight steps. First, a 0.4-μm thick chromium (Cr) film was deposited on the LNOI wafer using the magnetron sputtering method. Second, a layer of photoresist (PR) was spin-coated on the Cr film. After UV exposure and development, the circular patterns on the mask were transferred to the PR layer. Then, the Cr film without PR protection was etched up by ICP-RIE. Thus, the patterns were transferred to the Cr layer. Third, using Cr as a hard mask, the circular erbium-doped LN disks were formed via CMP. In the CMP process, a standard wafer polishing machine, polishing suspensions with silicon-dioxide grains, and a soft velvet polishing cloth were utilized. The Cr mask and the exposed LN film contacted with the polishing slurry due to the usage of the soft polishing cloth and the hundreds-of-nanometers height difference between the Cr film and LN layer. Cr (Mohs 9) is much harder than LN (Mohs 5); thus, the removal rate of the LN film is faster than that of the Cr film. Naturally, the circular patterns on the Cr layer were transferred to the erbium-doped LN layer. Meanwhile, the sidewalls of the erbium-doped LNOI microdisk cavities were

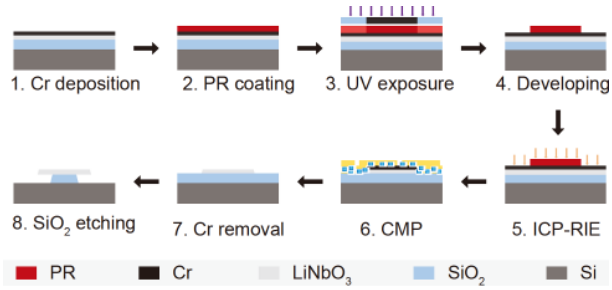

Figure 1 (Color online) Diagram of the fabrication process of erbium-doped LNOI microdisks. PR: photoresist; CMP: chemomechanical polishing; ICP-RIE: inductively coupled plasma reactive ion etching.

sufficiently polished to obtain smooth sidewalls and to reduce scattering losses. Finally, the fabricated sample was immersed in a Cr etching solution for 10 min to remove the remaining Cr layer. Subsequently, the silica was partially etched in a buffered hydrofluoric acid solution to achieve suspended erbium-doped LNOI microdisks for the convenience of coupling via tapered fiber.

The geometric and optical features of the fabricated erbium-doped LNOI microdisks were characterized. Figure 2(a) shows a typical optical micrograph of an erbium-doped LNOI microdisk cavity with a radius of 45 μm. Compared with undoped LNOI microdisks, the silica pillar has a noncircular shape because of the loose bonding between the silicon-dioxide layer and the LN film layer. As the etching time of buffered hydrofluoric acid increased, the silicon-dioxide layer eroded seriously, which might have introduced additional losses to the erbium-doped LNOI microdisk cavity and reduced the Q factor. The Q factors of the erbium-doped LNOI microdisk cavities in the 980-nm band were measured by fitting the transmission spectrum of the fiber-coupled microdisks. Figure 2(b) illustrates a typical transmission spectrum near 971.30 nm detected using the pump-wavelength scanning method. The black curves in the figure are the experimental data, whereas the green, red, and blue curves are fitted by Lorentzian function with different peaks. The loaded Q value is 1.25×10^6 for the under-coupled mode. In the under-coupling regime, the intrinsic Q factor is approximately equal to the loaded Q factor, whereas the

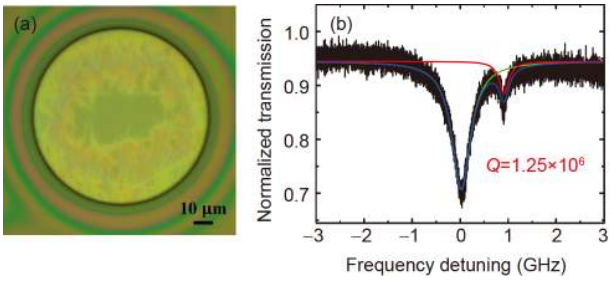

Figure 2 (Color online) (a) Optical micrograph of a typical erbium-doped LN microdisk cavity; (b) transmission spectrum showing the measured Q factors of the erbium-doped LN microdisk.

coupling loss can be neglected. The transmission spectrum in Figure 2(b) has double peaks, probably being the manifestation of mode splitting effect caused by particle scattering. The possible reason for the low Q value is the relatively strong absorption of erbium ions in the 980-nm band, which increases the intrinsic loss of an LN microcavity. On the basis of the measured Q factor of the erbium-doped LNOI microdisks, we estimated the erbium concentration to be 1.9×10^{25} ions m^{-3} in the case of a weak pump [27]. This concentration is close to the doping solubility of 0.1 mol% (1.5×10^{25} ions m^{-3}) of the erbium-doped LN crystal from which the LNOI film was sliced.

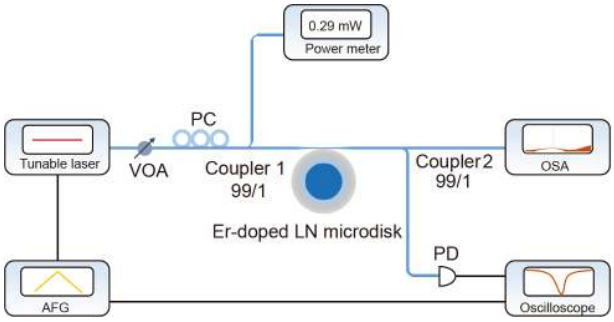

Figure 3 (Color online) Experimental setup for the observation of photoluminescence in erbium-doped LNOI microdisk cavities. AFG: arbitrary function generator; VOA: variable optical attenuator; PC: polarization controller; OSA: optical spectrum analyzer; PD: photodetector.

3 Laser in erbium-doped LNOI microdisks

To investigate the photoluminescence characteristics of the fabricated erbium-doped LNOI microdisks, we pumped the cavities using a tunable narrow-band laser operating at the 980-nm band. Figure 3 schematically illustrates the experimental setup. The pump laser first transmitted through an optical attenuator and a polarization controller and was then divided into two parts using the fiber coupler 1. The minor part (1%) was connected to a power meter to monitor the pump power in the optical path. The major part (99%), acting as the pump in the photoluminescence experiments, was evanescently coupled into the erbium-doped LNOI microdisk cavity through a tapered fiber with a waist approximately 1 μm in diameter. The erbium-doped LNOI microdisk was placed on a three-axis piezostage to precisely control the relative position of microdisk and the tapered fiber and thus their coupling. During the coupling process, the fiber was always attached to the microdisk to ensure the signal stability. The generated signal and transmitted pump were extracted by the same tapered fiber simultaneously. Similarly, through the fiber coupler 2, the output from the tapered fiber was also divided into two parts: 99% of the collected light was launched into an optical spectrum analyzer (OSA), which has a response wavelength of 600-1700 nm, to detect the 1550-nm band signal; 1% of the collected light was sent to a photodetector, and its output electrical signal was collected by an oscilloscope to monitor the transmission spectrum of the pump and thus its coupling state. Through the external driving function, that is, the sawtooth waveform voltage signal generated by AFG, the pump laser wavelength can be finely tuned. At the same time, AFG provides a trigger signal to the oscilloscope so that the transmission spectrum on the oscilloscope can be displayed stably. In our experiments, light signals at the 1550-nm band were detected from OSA when the pump laser was scanned in the 965-980-nm spectral range. Green upconversion fluorescence was observed in the meantime using a visible-light camera, as shown in Figure 4(a). As the input pump power increases, multiple signal peaks appear on both sides of the main signal. The reason is that the metastable state $^4I_{13/2}$ and the ground state $^4I_{15/2}$ of erbium ions are multiple degenerate states, which allow multiple signal peaks corresponding to energy levels in the 1550-nm band region, as illustrated in Figure 4(b). We also noticed the evolution of a signal spectrum at different pump power, as illustrated in Figure 4(c). At first, when the pump power was low, a broad, spontaneous emission gain background existed. Subsequently, with the increase in pump power, the laser signal began to emerge from the back of the fluorescence and the signal linewidth gradually narrowed. In principle, the signal linewidth should be consistent with that of the cavity mode (~0.001 nm). However, due to the limited resolution of OSA (0.01 nm), the actual linewidth of the signal was imperfectly reflected.

We decided to detect the signal intensity dependence around 1531.8 nm on the pump power. First, a 25-Hz, 2-V peak-peak sawtooth voltage generated by AFG was applied to the pump laser to adjust the pump wavelength and trace the pump mode corresponding to the signal. Second, AFG was turned off and the pump wavelength was manually adjusted to ensure the maximum signal gain at the given pump power by placing the pump mode in the deepest coupling region. Experimentally, the pump wavelength was tuned within the 974.31-974.79-nm spectral range. The signal power under different pump power was detected and is shown in Figure 4(d); the transmission loss of the components in the optical path was deducted. Due to the strong absorption of erbium ions in the pump band, erbium-doped LN microdisk has a strong thermo-optic effect. As a result, we could not achieve the effective lock of the pump mode at high pump power. Therefore, the stable value of the signal mode gain cannot be accurately obtained. However, an evident threshold exists for the variation of the signal power with the pump power, which confirms that the signal we observed is a laser rather than a spontaneous emission when the LNOI disk was pumped strongly. By linearly fitting the

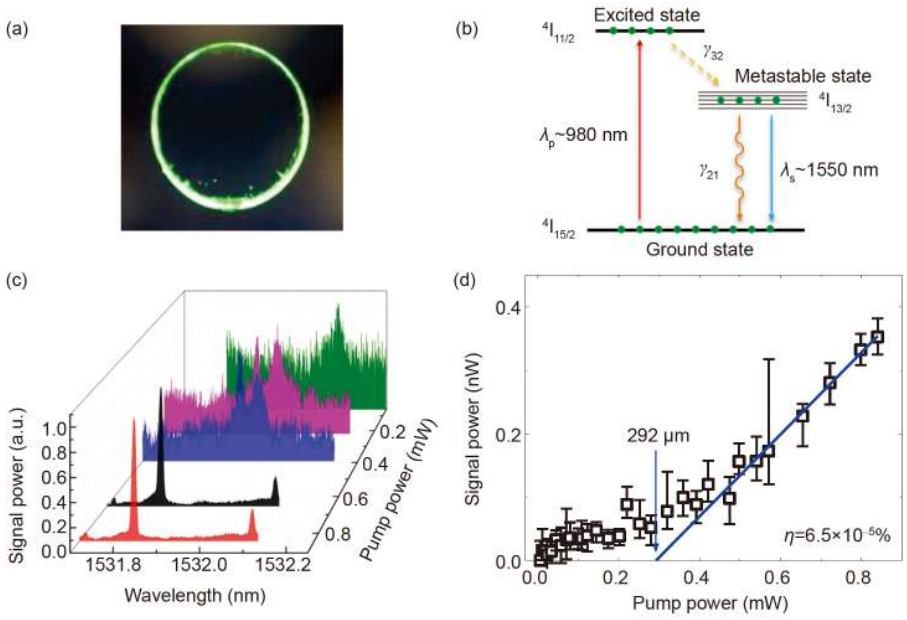

Figure 4 (Color online) (a) Optical image showing the green up-conversion fluorescence; (b) three-level system of erbium ions under the pump of a 980-nm laser; (c) spectrum evolution of the signal mode at different pump power; (d) dependence of the signal power on pump power, showing the threshold and conversion efficiency of an erbium-doped LNOI disk laser, which is approximately 1531.8 nm.

curve, we can obtain a laser threshold of 292 μW and a differential conversion efficiency of 6.5×10^{-5}%. In addition, the central wavelength of the signal laser mode can be continuously adjusted in the range of several GHz because of the thermal broadening of the pump mode [28].

In our experiment, the up-conversion process consumes a part of the pump energy so that the gain obtained by the signal in the 1550-nm band is reduced, thereby increasing the threshold of the signal laser. In addition, LNOI film undergoes a strong photorefractive effect under the 980-nm pump [29], creating a refractive index nonuniformity. This nonuniformity, in turn, causes the pump mode to evolve to a high-order mode, reducing the efficiency of the pump. As a result, the gain value of the signal is also reduced. In the later stage, MgO can be co-doped into erbium-doped LNOI film to suppress the photorefractive effect and to further reduce the signal laser threshold.

In the preparation of this paper, we found that two similar articles were posted on arXiv [30,31]. The difference between their work and ours is that our fabrication method can achieve high-quality-factor erbium-doped LN microdisk in batch, which is more efficient and can benefit the practical applications of on-chip LNOI lasers.

4 Conclusions

In summary, on-chip erbium-doped LN high-Q microdisk cavities were fabricated by UV exposure, inductively coupled plasma reactive ion etching, and chemomechanical polishing, allowing for batch processing. Under the pump of a continuous-wave laser in the 980-nm band, the laser operation at 1550-nm band was realized. The laser threshold was approximately 292 μW, and the differential efficiency was 6.5×10^{-5}%. This work will alleviate the shortage of laser sources of the LNOI integrated platform and will propel the development of integrated photonics based on LNOI.

This work was supported by the National Key Research and Development Program of China (Grant No. 2019YFA0705000), the National Natural Science Foundation of China (Grant Nos. 12034010, 11734009, 11674181, 11674184, and 11774182), the Higher Education Discipline Innovation Project (Grant No. B07013), the National Science Fund for Talent Training in the Basic Sciences (Grant No. J1103208), and the Program for Changjiang Scholars and Innovative Research Team in University (PCSIRT) (Grant No. IRT_13R29).

1 T. A. Ramadan, M. Levy, and R. M. Osgood Jr., Appl. Phys. Lett. **76**, 1407 (2000).
2 J. Lin, Y. Xu, Z. Fang, M. Wang, J. Song, N. Wang, L. Qiao, W. Fang, and Y. Cheng, Sci. Rep. **5**, 8072 (2015).
3 C. Wang, M. J. Burek, Z. Lin, H. A. Atikian, V. Venkataraman, I. C. Huang, P. Stark, and M. Lončar, Opt. Express **22**, 30924 (2014), arXiv: 1410.2625.
4 J. Wang, F. Bo, S. Wan, W. Li, F. Gao, J. Li, G. Zhang, and J. Xu, Opt. Express **23**, 23072 (2015).
5 R. Wu, J. Zhang, N. Yao, W. Fang, L. Qiao, Z. Chai, J. Lin, and Y. Cheng, Opt. Lett. **43**, 4116 (2018), arXiv: 1806.00099.
6 J. Zhang, Z. Fang, J. Lin, J. Zhou, M. Wang, R. Wu, R. Gao, and Y. Cheng, Nanomaterials **9**, 1218 (2019).
7 M. Wang, R. Wu, J. Lin, J. Zhang, Z. Fang, Z. Chai, and Y. Cheng, Quantum Eng. **1**, e9 (2019).

8 Z. Hao, J. Wang, S. Ma, W. Mao, F. Bo, F. Gao, G. Zhang, and J. Xu, Photon. Res. **5**, 623 (2017).
9 Z. Z. Hao, L. Zhang, A. Gao, W. B. Mao, X. D. Lyu, X. M. Gao, F. Bo, F. Gao, G. Q. Zhang, and J. J. Xu, Sci. China-Phys. Mech. Astron. **61**, 114211 (2018).
10 C. Wang, C. Langrock, A. Marandi, M. Jankowski, M. Zhang, B. Desiatov, M. M. Fejer, and M. Lončar, Optica **5**, 1438 (2018).
11 R. Wolf, Y. Jia, S. Bonaus, C. S. Werner, S. J. Herr, I. Breunig, K. Buse, and H. Zappe, Optica **5**, 872 (2018), arXiv: 1803.10577.
12 J. Lin, N. Yao, Z. Hao, J. Zhang, W. Mao, M. Wang, W. Chu, R. Wu, Z. Fang, L. Qiao, W. Fang, F. Bo, and Y. Cheng, Phys. Rev. Lett. **122**, 173903 (2019).
13 J. Lu, J. B. Surya, X. Liu, A. W. Bruch, Z. Gong, Y. Xu, and H. X. Tang, Optica **6**, 1455 (2019), arXiv: 1911.00083.
14 Z. Hao, L. Zhang, W. Mao, A. Gao, X. Gao, F. Gao, F. Bo, G. Zhang, and J. Xu, Photon. Res. **8**, 311 (2020).
15 X. Ye, S. Liu, Y. Chen, Y. Zheng, and X. Chen, Opt. Lett. **45**, 523 (2020).
16 L. Zhang, Z. Hao, Q. Luo, A. Gao, R. Zhang, C. Yang, F. Gao, F. Bo, G. Zhang, and J. Xu, Opt. Lett. **45**, 3353 (2020).
17 Y. He, Q. F. Yang, J. Ling, R. Luo, H. Liang, M. Li, B. Shen, H. Wang, K. Vahala, and Q. Lin, Optica **6**, 1138 (2019), arXiv: 1812.09610.
18 C. Wang, M. Zhang, X. Chen, M. Bertrand, A. Shams-Ansari, S. Chandrasekhar, P. Winzer, and M. Lončar, Nature **562**, 101 (2018).
19 M. He, M. Xu, Y. Ren, J. Jian, Z. Ruan, Y. Xu, S. Gao, S. Sun, X. Wen, L. Zhou, L. Liu, C. Guo, H. Chen, S. Yu, L. Liu, and X. Cai, Nat. Photon. **13**, 359 (2019), arXiv: 1807.10362.
20 L. Cai, and G. Piazza, J. Opt. **21**, 065801 (2019).
21 A. Kar, M. Bahadori, S. Gong, and L. L. Goddard, Opt. Express **27**, 15856 (2019).
22 I. Krasnokutska, J.-L. J. Tambasco, and A. Peruzzo, Opt. Express **27**, 16578 (2019).
23 N. Yao, J. Zhou, R. Gao, J. Lin, M. Wang, Y. Cheng, W. Fang, and L. Tong, Opt. Express **28**, 12416 (2020), arXiv: 2002.09206.
24 S. Wang, L. Yang, R. Cheng, Y. Xu, M. Shen, R. L. Cone, C. W. Thiel, and H. X. Tang, Appl. Phys. Lett. **116**, 151103 (2020), arXiv: 1912.07584.
25 S. Dutta, E. A. Goldschmidt, S. Barik, U. Saha, and E. Waks, Nano Lett. **20**, 741 (2020), arXiv: 1911.06376.
26 D. Pak, H. An, A. Nandi, X. Jiang, Y. Xuan, and M. Hosseini, J. Appl. Phys. **128**, 084302 (2020).
27 B. Min, T. J. Kippenberg, L. Yang, K. J. Vahala, J. Kalkman, and A. Polman, Phys. Rev. A **70**, 033803 (2004).
28 Z. Chen, X. Tu, J. Zhao, and H. Y. Fu, IEEE Photon. Technol. Lett. **31**, 1650 (2019).
29 C. H. Huang, and L. McCaughan, IEEE J. Sel. Top. Quantum Electron. **2**, 367 (1996).
30 Z. Wang, Z. Fang, Z. Liu, W. Chu, Y. Zhou, J. Zhang, R. Wu, M. Wang, T. Lu, and Y. Cheng, arXiv: 2009.08953.
31 Y. A. Liu, X. S. Yan, J. W. Wu, B. Zhu, Y. P. Chen, and X. F. Chen, Sci. China-Phys. Mech. Astron. **64**, 234262 (2021), arXiv: 2009.12900.